PREDICTION OF IMPACT DAMAGE ON DOUBLE BUMPER SHIELDS FOR THE PROTECTION OF ORBITING MANNED MODULES

David Palmieri[(1)], Michel Lambert[(2)]

[(1)]ESA-ESTEC, Postbus 299, 2200 AG, Noordwijk, The Netherlands, David.Palmieri@esa.int
[(2)]ESA-ESTEC, Postbus 299, 2200 AG, Noordwijk, The Netherlands, Michel.Lambert@esa.int

ABSTRACT

Hypervelocity impacts of space debris, represented by aluminium spheres, against typical shielding systems for the International Space Station (ISS) manned modules are simulated using the AUTODYN-2D hydrocode. The considered shield type is the *double bumper shield*, i.e., two separate bumpers placed in front of the structure to be protected.
Numerical tools are first tested and calibrated through the simulation of available tests, at the maximum impact velocity currently attainable (around 6.5 km/s). As the estimated debris average impact velocity along the ISS orbit is around 10 km/s, the model giving the best agreement with the experiments is then used for the ballistic limit extrapolation in the velocity range not experimentally achievable. The results of numerical extrapolation are compared with the semi-empirical curves actually used for the ballistic limit estimation in the high velocity regime, based on the assumption of damage proportional to projectile momentum.

1. INTRODUCTION

The International Space Station (ISS) manned modules are actually protected from the Meteoroids and Orbital Debris (M/OD) threat using two basic shield configurations. A simple aluminium thin bumper (*Whipple shield*) is located in front of the less exposed areas to the M/OD environment, while an intermediate composite bumper is added at a given distance between the first one and the main structure (*double bumper shield*) where the maximum probability of high energy impacts is expected. On the European laboratory Columbus double bumper shields are placed in front of the Cylinder Forward, Port Cone Forward and Starboard Cone sections [1].
The estimated average impact velocity of debris along the ISS orbit is around 10 km/s. The main limitation in the shields design is the assessment of ballistic performances at impact velocities higher than about 7 km/s. The largest masses of objects against which a shielding protection is required (order of grams) cannot be accelerated beyond this limit by the currently available experimental techniques (mainly Light Gas Gun, LGG). Therefore, numerical and/or analytical tools are required to predict the shields ballistic limit in the higher velocity regime.
The performances of Whipple shields have been extensively studied, and the ballistic limit at the highest velocities is currently assessed with enough confidence through both semi-empirical equations [2] and hydrocodes simulations [3].
On the other hand, the use of theoretical and numerical models for the extrapolation of double bumper shields ballistic limit is actually affected by higher uncertainties [4]. More complex physical phenomena are involved in the impact process due to the addition of a second bumper in front of the structure. Furthermore, in most of ISS modules the second bumper is made of advanced material such as Nextel and Kevlar, whose behaviour models at very high strain rates were only recently developed [5] and have not been extensively tested yet.
The simulation of some LGG impact tests on the specimens representing the Columbus double bumper shields (*Advanced Shields*, AS), and the extrapolation of the target ballistic limit in the higher velocity range are described in the following sections. The work was performed to support the validation of the Columbus M/OD Protective System (MDPS).

2. TARGET CONFIGURATION AND TESTS

The Columbus AS configuration selected for the numerical simulations is that protecting the Cylinder Forward section, shown in Fig. 1.

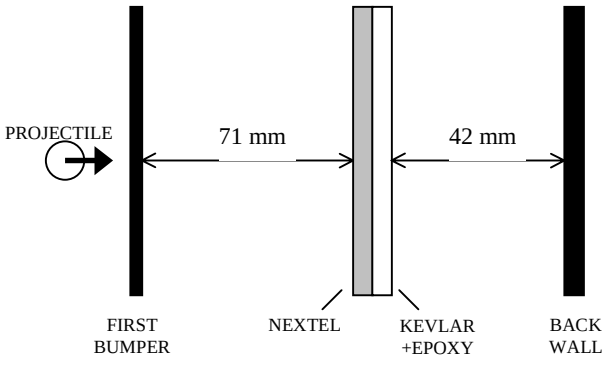

Fig. 1. Columbus Cylinder Forward shield

The 2.5 mm first bumper is made of Al6061-T6. The second bumper is composed by 4 mm of Nextel 312 style AF62 fabric layers, placed on top of 6 mm of

Kevlar 129 style 812 fabric layers impregnated with epoxy resin 912 to a mass rate of 40%. The 4.8 mm Al2219-T851 back wall represent the pressurised module shell.
The final objective of numerical analysis is the ballistic limit extrapolation in the impact velocity range not experimentally achievable, based on a previous model calibration through the comparison with available tests. Therefore, the experimental impact conditions closer to the required extrapolation range were selected for the calibration of numerical model, i.e., LGG tests at the maximum available impact velocity (around 6.5 km/s). The simulated tests, performed at Ernst Mach Institut (Freiburg, Germany) [6], are reported in Table 1. In all cases the projectile was a Al2007 sphere.

Table 1. Simulated LGG tests

TEST NR.	IMPACT VEL. (m/s)	PROJECTILE DIAM. (mm)	BACK WALL PERFORATION
8603	6500	14.5	NO
8611	6510	15	YES (cracks)*
8602	6580	15.5	YES (hole)

(*) damage condition close to the ballistic limit

If all aluminium shields are considered, the eventual back wall perforation is generally identified by the presence of a net hole. This is not the case of Columbus AS, whose principal damage mode is due to the impulsive load delivered on the back wall, rather than to the action of individual fragments producing craters and/or holes. The AS back wall perforation criterion, i.e., a damage condition exceeding the ballistic limit, was the presence of at least one crack permeable to creeping fluid. In most cases where a perforation was assessed according to the selected criterion, it was due to cracks opening, without any net perforation hole. This was also the case of test 8611, that was classified as a perforation, but the back wall damage condition was reported to be very close to the threshold limit. The selected tests allow a good estimation of the Columbus AS ballistic limit at 6.5 km/s, that can be located around 15 mm or slightly below.

3. SIMULATIONS

3.1 Geometry and spatial resolution

Simulations were performed with AUTODYN-2D in axial symmetry. With the use of axial symmetry it is possible to simulate normal impacts with a 2D model, thus allowing a consistent saving in terms of computation time. However, this model cannot reproduce asymmetric features such as the radial cracks observed in the Columbus AS specimens. On the other hand, the use of a complete 3D model would have requested an excessively long computation time.

The projectile and the two bumpers were represented with the SPH technique, while the back wall was represented by a Lagrange grid together with an erosion algorithm. The spatial resolution was chosen to have 10 particles through the 1st bumper thickness, with a dimension of 0.25 mm. In order to keep the same particles and Lagrange cells dimension in the whole model, 16 and 24 SPH particles were used through the thickness of Nextel and Kevlar-epoxy respectively, while 19 Lagrange cells were placed through the back wall thickness.
The two bumpers were modelled with a radial extension lower than in the experiments but enough to catch all the impacting material, in order to decrease the nodes number and reduce the computation time. However, the impact dynamics on the two bumpers is very fast, and boundary effects can be neglected. On the other hand, the back wall is subjected to large plastic deformation, and its extension was considered important for the assessment of the overall damage. In test samples it was represented by a rectangular plate 400x600 mm, but in a 2D axial symmetric model is only possible to represent circular plates. The back wall diameter was set to 400 mm, equal to the minimum dimension of test samples, and the radial dimension of Lagrange cells was progressively increased far from the symmetry axis.

3.2 Material models

The shock Equation Of State (EOS) was used for the aluminium alloys. The Al2007 projectile and the Al2219-T851 back wall were represented with the Johnson-Cook strength model, and due to the lack of data for these materials, the numerical parameters for Al2024-T351 were used. The Steinberg-Guinan strength model for Al6061-T6 was available from the AUTODYN library, and it was used to represent the 1st bumper. The principal stress failure criterion was used for all the aluminium parts of the model.
Nextel and Kevlar-epoxy were represented with the AMMHIS material model, that was specifically developed for this application [5]. The AMMHIS validation analysis suggested to represent Nextel with an isotropic model and Kevlar-epoxy with an orthotropic equation of state.

3.3 Simulation of LGG tests

The aim of the comparison between experiments and simulations is to gain confidence in the numerical prediction of ballistic limit. Test 8611 gives a back wall damage condition very close to the perforation threshold, and therefore it was selected as a main reference for the calibration of numerical model.
The spatial resolution was kept constant throughout the analysis as well as the artificial viscosity coefficients, for which the AUTODYN default value of 1 was used.

In the first simulation case (S8611a) the principal stress tensile limit for all aluminium alloys was set at 1.2 GPa, as this value is commonly adopted in the open literature. The post-failure behaviour of Kevlar-epoxy was modelled using the isotropic option [5]. The back wall was not perforated, with a predicted residual thickness of 2.7 mm, i.e., 56% of the initial value (see Fig. 2, left side). Such a damage condition can be considered quite far from the ballistic limit.

In order to try improving the correlation with the experiments, the failure stress of aluminium alloys was changed according to the failure criterion proposed by Grady [7]. This criterion states that if a given material is subjected to a strain rate higher than a critical value $\dot{\varepsilon}_c$, the failure stress σ_R is independent of the strain rate (ductile spall), and it is given by

$$\sigma_R^{(d)} = (2\rho c_0^2 Y v_f)^{1/2} \tag{1}$$

while the value of the critical strain rate is

$$\dot{\varepsilon}_c = \left(\frac{8}{9} \frac{B_0^2 (Y v_f)^3}{\rho K_c^4} \right)^{1/2} \tag{2}$$

where

ρ = density
c_0 = elastic waves soundspeed
Y = yield stress
v_f = critical voids volume fraction (assumed 0.15)
B_0 = bulk modulus = ρc_0^2
K_c = fracture toughness

On the other hand, if the strain rate $\dot{\varepsilon}$ applied to the material is lower than $\dot{\varepsilon}_c$ the failure stress depends on $\dot{\varepsilon}$ (brittle spall), and it can be calculated from

$$\sigma_R^{(b)} = (3\rho c_0 K_c^2 \dot{\varepsilon})^{1/3} \tag{3}$$

The average strain rate at which the three aluminium components are subjected in test 8611 was obtained from the simulations, and is reported in Table 2 together with the corresponding critical strain rate and failure stress calculated according to the Grady's criterion.

The simulation of test 8611 with the aluminium alloys failure stresses reported in Table 2 (S8611b) resulted again in the no perforation of back wall, with a residual thickness of 1.6 mm (33% of the initial value). A small zone of failed material within the remaining portion of the plate thickness was observed (see Fig. 2, center).

Table 2: aluminium failure parameters (test 8611)

MATERIAL	$\dot{\varepsilon}$ (s^{-1})	$\dot{\varepsilon}_c$ (s^{-1})	FAILURE STRESS (GPa)
PROJECTILE	$3 \cdot 10^6$	$3.2 \cdot 10^5$	2.34 (ductile)
1ST BUMPER	$3 \cdot 10^6$	$3.8 \cdot 10^5$	2.38 (ductile)
BACK WALL	$1 \cdot 10^5$	$3.7 \cdot 10^5$	1.77 (brittle)

The greater damage with respect to case S8611a, giving a condition closer to the ballistic limit, is due to the higher material density in the debris cloud after the shock release. In fact, the considerably higher failure stress of the projectile and first bumper increases the material load bearing capability, and such effect is prevailing over the increase of the back wall strength.

In the third simulation case (S8611c) the orthotropic post failure option for Kevlar-epoxy [5] was introduced. Again a back wall no perforation was obtained, with a residual thickness of 1.4 mm (29% of the initial value). The failed zones within the remaining part of the plate thickness are larger than in case S8611b, and a detached spall over a length of 0.7 mm on the rear face can also be observed (see Fig. 2, right side). In this case the damage increase was due to the higher density of Kevlar-epoxy impacting the back wall. In fact, the orthotropic post failure option allows the material to fail only in one direction, thus increasing the overall load bearing capability that is maintained in the other directions.

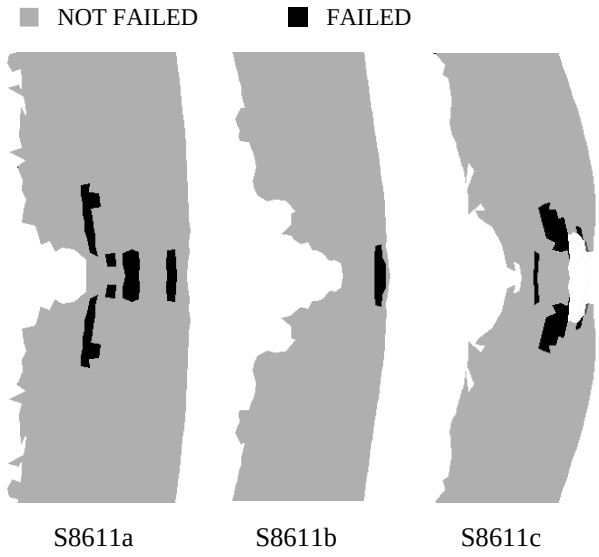

Fig. 2. Predicted back wall damage for test 8611 (Lagrange back wall, principal stress failure)

Even if close to the target ballistic limit, the result of test 8611 was classified as a perforation. In the attempt of obtaining this condition in the numerical analysis, test 8611 was simulated by modelling also the back wall with SPH particles (case S8611d). The particles size

was the same for the whole model (0.25 mm), so that 19 particles were set through the back wall thickness. A 62 mm perforation hole caused by the detachment of large material portions was obtained (see Fig. 3, left side). This failure mode is clearly due to the problem of numerical fracture, characteristic of the SPH technique. Such problem occurs when the distance among particles is higher than the selected interaction radius (*smoothing length*), and therefore the load is not transmitted through the material even if no failure criterion is exceeded.
The perforation observed in case S8611d is very far from a damage condition close to the ballistic limit, as observed in the experiments. Nevertheless, a simulation with SPH back wall was also performed for test 8603, in which a clear no perforation was reported. Even in this case (S8603d) a large perforation hole in the back wall was obtained (see Fig. 3, right side), thus confirming the limitations of SPH to adequately reproduce the back wall damage. On the other hand, SPH is not the most adequate technique to represent the behaviour of structures subjected to relatively low velocity impact and large plastic deformation, such as the back wall of Columbus AS.

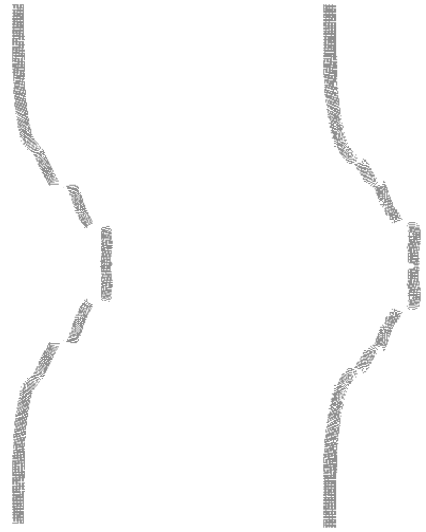

S8611d S8603d

Fig. 3. SPH back wall simulations

In order to try further improving the correlation of simulations with the experiments, the numerical model with a Lagrange back wall was modified by introducing a principal strain criterion for aluminium alloys, in addition to the principal stress criterion. In this way the material failure occurs when either the stress or the strain limit is first reached. Due to the lack of specific data for failure strain at high strain rates, the values reported in Table 3 taken from the open literature [8] were used.

Simulation of test 8611 (case s8611e) resulted in a large perforation hole through the back wall (see Fig. 4, left side). Even if the target perforation was achieved, the damage appeared too far from a condition close to the ballistic limit, in a similar manner as observed in the simulation with the SPH back wall.

Table 3: aluminium alloys failure strain

MATERIAL	Al2007 (projectile)	Al6061-T6 (1st bumper)	Al2219-T851 (back wall)
FAILURE STRAIN	0.07	0.12	0.1

The model was also used to simulate 8603 (case S8603e), and a clear target perforation was observed anyway (see Fig. 4, right side). From these results the use of the principal strain criterion seems to give a too weak representation of the back wall strength.

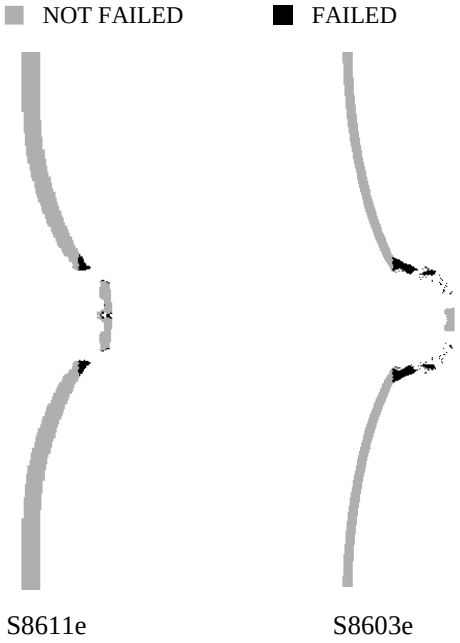

Fig. 4. Principal stress/strain failure simulations

The above described simulations of test 8611 did not allow to obtain a back wall perforation reasonably representing a damage condition close to the ballistic limit, as was observed in the experiment. On the other hand, it was already pointed out that the perforation resulting from test 8611 was not due to a net hole through the plate thickness, but to radial cracks that cannot be reproduced by the 2D numerical model.
Nevertheless, the back wall damage obtained in case S8611c (crater plus detached spall, residual wall thickness 29% of the initial one) can be considered as a quite good approximation of a condition close to the

ballistic limit, even if with a slight damage underestimation.
The numerical model of case S8611c was also used to simulate test 8603, where a clear no perforation was observed, and test 8602, where an evident perforation occurred. The results were in good agreement with the experiments, showing a no perforation with a residual thickness of 2.6 mm for test 8603 (case S8603c, Fig. 5, left side) and a perforation with a hole diameter of 3.1 mm for test 8602 (case S8602c, Fig. 5, right side). The final result of case S8611c is reported again in Fig. 5, in order to show the variation of the predicted back wall damage with the projectile diameter for the selected experiments.
Therefore, the ballistic limit of the Columbus AS predicted by the simulations at 6.5 km/s is between 15 mm (case S8611c, no perforation) and 15.5 mm (case S8602c, perforation). If it is located at a distance from the no perforation case proportional to the ratio between the back wall residual and initial thickness (see [3]), a value of 15.14 mm is obtained, thus giving an overestimation around 1% on the projectile diameter with respect to the experimental value.

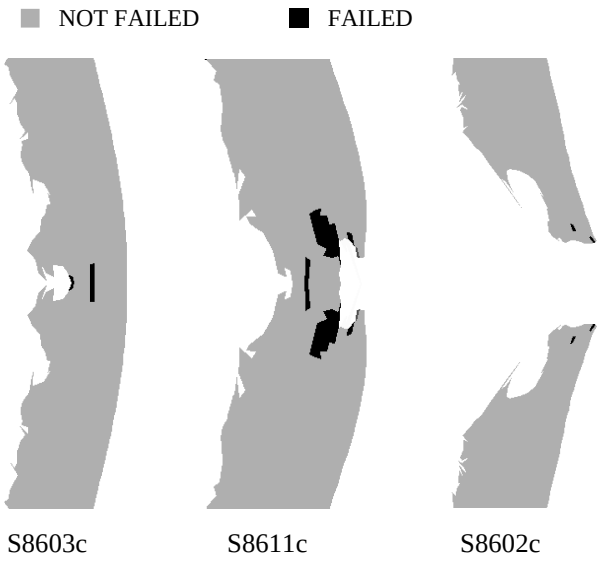

Fig. 5. Simulation of back wall damage at 6.5 km/s

3.4 Extrapolation at high impact velocities

The numerical model used in cases S8603c, S8611c and S8602c, was considered to give the best matching with LGG tests. Therefore, it was selected to predict the target ballistic limit at impact velocities higher than 6.5 km/s, not achievable with the current experimental techniques. The back wall failure stress was changed according to Eq. 3. The material applied strain rate, varying with the impact velocity V, was calculated from the simulations as reported in Table 3.

Table 3: back wall failure stress

V (km/s)	$\dot{\varepsilon}$ (s^{-1})	FAILURE STRESS (GPa)
8	$1 \cdot 10^5$	1.77 (brittle)
9.5	$2 \cdot 10^5$	2.24 (brittle)
11	$1.3 \cdot 10^5$	1.94 (brittle)

It is interesting to note the decreasing of the strain rate in the back wall when the impact velocity increases from 9.5 to 11 km/s. It has been calculated that at an impact velocity around 10.5 km/s aluminium should undergo a liquid-vapour phase transition [9]. Even if the shock EOS does not include any specific formulation for phase transitions, the largest material expansion following a more intense shock wave seems anyway able to simulate this kind of phenomenon. This behaviour was already observed in the prediction of Whipple shields ballistic limit [3].
For each impact velocity the projectile diameter was varied by 0.5 mm, until the back wall perforation and no perforation were obtained with two close values. The ballistic limit was then located between such values, at a distance from the no perforation point proportional to the ratio between the back wall residual and initial thickness.
The numerical results were compared with the semi-empirical curves actually used for the ballistic limit estimation in the high velocity regime, based on the assumption of damage proportional to projectile momentum. The relationship giving the ballistic limit D_C (expressed in cm) as a function of the impact velocity V (expressed in km/s) for the selected target, normal impacts and $V \geq 6.5$ is

$$D_C = 2.75 \cdot V^{-1/3} \tag{4}$$

The results of simulations are shown in Fig. 6 together with the curve calculated from Eq. 4. The results of LGG tests at 6.5 km/s are also reported.
Simulations predict an higher ballistic limit with respect to the semi-empirical curve for impact velocities ranging from 6.5 to about 9 km/s, while a slightly lower value is predicted between approximately 9 and 10 km/s. Above 10 km/s the curve obtained from simulations shows the upward trend already observed for Whipple shields [3], that is not taken into account by the semi-empirical equation and can be justified by the starting of aluminium vaporisation.
The maximum difference between the two curves is around 8 km/s, where simulations predict a ballistic limit about 7% higher than the semi-empirical curve. The two curves are closer in the range where numerical predictions are below the semi-empirical values, with a maximum difference of about 3% around 9 km/s.

This difference is assessed as being reasonably small compared with the uncertainties observed so far with hypervelocity impacts simulations.

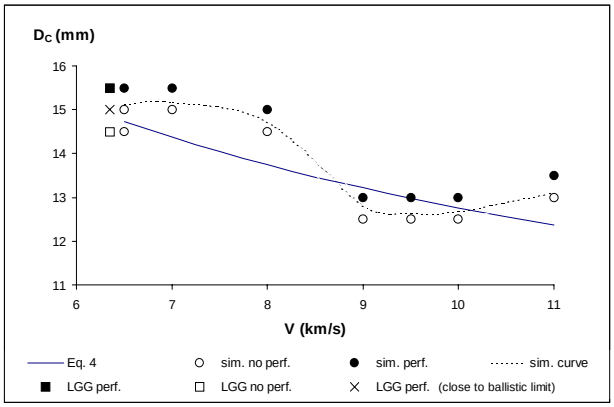

Fig. 6. Comparison of ballistic limit prediction by simulations and semi-empirical equations

4. CONCLUSIONS AND DEVELOPMENTS

LGG tests on the Columbus AS at impact velocities around 6.5 km/s were simulated using the AUTODYN-2D hydrocode, with the aim of calibrating the numerical model on the experimental results and use it for the ballistic limit prediction in the higher velocity regime, not currently attainable by experimental techniques.
The variation of the back wall failure stress according to the material applied strain rate and the use of Kevlar-epoxy orthotropic post-failure behaviour improved the correlation with tests, while modelling the back wall with SPH or principal stress/strain failure did not give satisfactory results. The results of selected model were in good agreement with the experiments, even if the final back wall damage was slightly underestimated.
The numerical ballistic limit extrapolation at higher velocities was close to the semi-empirical equations based on the assumption of damage proportional to projectile momentum. The difference between the two curves did not exceed 7% on the projectile diameter, corresponding to about 20% on mass.
The confidence gained in the 2D simulations of normal impacts will be useful in the 3D analysis of oblique impacts, that will be necessarily limited by the very high computation times. The simulation of shaped charge impact tests and the analysis of projectile shape effects is also foreseen.

ACKNOWLEDGEMENTS

The authors acknowledge the Columbus project for the support received during the realisation of the work.

REFERENCES

1. Beruto E., Destefanis R., Faraud M. and Buchwald P., High resistance debris shielding development for the Columbus Orbital Facility, *Proceedings of the Second European Conference on Space Debris*, Darmstadt, Germany, 17-19 March, 1997, pp. 509-517.

2. Christiansen E.L. and Kerr J.H., Ballistic Limit Equations for Spacecraft Shielding, *Hypervelocity Impact Symposium 2000*, Galveston, TX, November 6-10.

3. Palmieri D., Faraud M., Destefanis R. and Marchetti M., Whipple Shield Ballistic Limit at Impact Velocities higher than 7 km/s, *Hypervelocity Impact Symposium 2000*, Galveston, TX, November 6-10.

4. Destefanis R., Faraud M., Palmieri D. and Marchetti M., SPH Simulations of Debris Impacts Using two Different Computer Codes, *International Journal of Impact Engineering*, Vol. 23, Nr. 1, December 1999, pp. 249-260.

5. Hiermaier S., Riedel W., Hayhurst C.J., Clegg R.A. and Wenzel C.M., Advanced Material Models for Hypervelocity Impact Simulations, *ESTEC Contract 12400/97/NL/PA(SC), Final Report*.

6. Hypervelocity Impact Test Campaign 1997, EMI-HVITC 003.

7. Grady D.E., The spall strength of condensed matter, *J. Mech. Phys. Solids*, Vol. 36, No. 3, pp. 353-384, 1988.

8. MIL-HDBK-5.

9. Schmidt R. M., Housen K. R., Piekutowski A. J. and Poormon K. L., Cadmium Simulation of Orbital-Debris Shield Performance to Scaled Velocities of 18 km/s, *Journal of Spacecraft and Rockets*, Vol. 31, No. 5, September-October 1994, pp. 866-877.